MITSUBISHI ELECTRIC RESEARCH LABORATORIES
http://www.merl.com

A Hamiltonian Approach to Compute an Energy Efficient Trajectory for a Servomotor System

Wang, Y.; Ueda, K.; Bortoff, S.A.

TR2013-104 December 2013

Abstract

This paper considers a nonlinear constrained optimal control problem (NCOCP) originated from energy optimal trajectory planning of servomotor systems. Solving the exact optimal solution is challenging because of the nonlinear and switching cost function, and various constraints. This paper proposes a method to manage the switching cost function to establish a set of necessary conditions of an NCOCP. Specifically, a concept "sub-trajectory" is introduced to match multiple Hamiltonian due to switches in the cost function. Necessary conditions on the optimal trajectory is established as a union of conditions for all sub-trajectories and Weierstrass-Erdmann corner conditions between sub-trajectories. The set of feasible structures of optimal trajectories is further identified and represented by various state transition diagrams for the servomotor application. A decomposition-based shooting method is proposed to compute an optimal trajectory by solving multi-point boundary value problems. Simulations and experiments validate the effectiveness of the methodology and the energy saving benefit.

Automatica

A Hamiltonian approach to compute an energy efficient trajectory for a servomotor system ⋆

Yebin Wang [a], Koichiro Ueda [b], Scott A. Bortoff [a]

[a] *Mitsubishi Electric Research Laboratories, 201 Broadway, Cambridge, MA 02139, USA*

[b] *Advanced Technology R&D Center, Mitsubishi Electric Corporation, 8-1-1, Tsukaguchi-honmachi, Amagasaki City, 661-8661, Japan*

Abstract

This paper considers a nonlinear constrained optimal control problem (NCOCP) originated from energy optimal trajectory planning of servomotor systems. Solving the exact optimal solution is challenging because of the nonlinear and switching cost function, and various constraints. This paper proposes a method to manage the switching cost function to establish a set of necessary conditions of an NCOCP. Specifically, a concept "sub-trajectory" is introduced to match multiple Hamiltonian due to switches in the cost function. Necessary conditions on the optimal trajectory is established as a union of conditions for all sub-trajectories and Weierstrass-Erdmann corner conditions between sub-trajectories. The set of feasible structures of optimal trajectories is further identified and represented by various state transition diagrams for the servomotor application. A decomposition-based shooting method is proposed to compute an optimal trajectory by solving multi-point boundary value problems. Simulations and experiments validate the effectiveness of the methodology and the energy saving benefit.

Key words: optimal trajectory, servomotors, constraints, switching functions

1 Introduction

Trajectory planning, together with path planning, are two major steps in a wide range of applications, for instance motion control in factory automation systems, aircrafts, robotics, unmanned aerial vehicles etc. A reference trajectory shall not only define the speed pattern to meet certain performance, but also have a smooth profile to avoid exciting natural modes of a plant. A majority of existing work focus on the time optimal trajectory planning in order to maximize a plant's productivity for instance, Lambrechts et al. (2005); Toacse and Culpi (1976); Park and Won (1991); La-orpacharapan and Pao (2004); Vasak et al. (2007) etc. The time optimal or approximate time optimal trajectory generation have been intensively studied in the past decades and result in numerous sound work including dynamic programming approach Shin and Mckay (1986); Singh and Leu (1987), minimum principle approach Chang (1963); Bobrow et al. (1985); Shiller and Lu (1992); Shin and Mckay (1985), optimization-based approach Verscheure et al. (2009) etc. A time optimal trajectory is not always desirable because it disregards the energy consumption of the motion control system, and can lead to a high peak power as well as a waste of energy.

Another important criteria to generate a reference trajectory is the energy consumption. This is practically meaningful in factory automation due to the fact that motion control systems consume approximately 65% of the electricity in industry Worrell et al. (2009). Work in this area includes the motor system steady state energy optimization Abrahamsen et al. (1998); Ghozzi et al. (2004), energy-optimal control scheme for incremental motion drive Trzynadlowski (1988); Sheta et al. (2009), a heuristic approach Dodds (2008); Vittek et al. (2010). Work Trzynadlowski (1988); Sheta et al. (2009); Dodds (2008); Kim and Kim (2007) does not address speed and acceleration constraints thus leads to a conservative design. Work Zhao et al. (2013) considers various constraints but with a smooth quadratic cost function thus conventional minimum principle is applied.

This paper focus on the energy optimal trajectory planning for a motion control system comprising a servomo-

⋆ This paper was not presented at any IFAC meeting. Corresponding author Y. Wang. Tel. +1-617-621-7500. Fax +1-617-621-7550.

Email addresses: yebinwang@ieee.org (Yebin Wang), Ueda.Koichiro@da.MitsubishiElectric.co.jp (Koichiro Ueda), bortoff@merl.com (Scott A. Bortoff).

tor as an actuator. Particularly, the motion control system is performing a single-axis point to point positioning task. A reference trajectory is generated to minimize a cost function reflecting a trade-off between the energy consumption and tracking time. Minimizing the cost function subject to various constraints is posed as a nonlinear constrained optimal control problem (NCOCP).

The difficulty to obtain the analytical solution of an NCOCP is well understood, and seeking a numerical solution has been an important topic for decades. Numerical methods for trajectory planning are usually categorized into direct Verscheure et al. (2009); Elnagar et al. (1995); Fahroo and Ross (2000); Gong et al. (2006) and indirect methods Shin and Mckay (1986); Bobrow et al. (1985); Shin and Mckay (1985). Model predictive control technique has been applied to solve free final time trajectory planning Richards and How (2003); Shim et al. (2003); Singh and Fuller (2001), while its application to fixed final time problems is limited. Direct methods represents a large class of algorithms which discretize an NCOCP into a mathematical programming problem over finite dimensional parameter space. Direct collocation Verscheure et al. (2009); Ascher et al. (1981) and pseudo-spectral Elnagar et al. (1995); Fahroo and Ross (2000) are two main techniques used in the discretization. Indirect methods resort to solve necessary conditions derived from the Minimum Principle Pesch (1989); Gergaud and Haberkorn (2006); Pesch (1994), which usually ends up with boundary value problems. Compared to indirect methods, direct methods have advantages in capabilities to handle complicated constraints and performance metrics, and having relative robustness to initial guesses. It however suffers from issues such as convergence speed and low accuracy of solutions, especially for cases where optimal solutions switch. Pseudo-spectral methods improves the convergence speed but assumes optimal solutions are smooth. Indirect methods usually yield a solution with very high accuracy Pesch (1994) but requires the structure of the optimal solution as a *priori*. Limitations of indirect methods includes two folds: the derivation of necessary conditions is not always easy Gong et al. (2006); the determination of the structure information of the optimal solution is usually difficult. Recent work Verscheure et al. (2009) formulates a class of NCOCP as a convex optimization problem. However Verscheure et al. (2009) assumes a model without viscous friction, and does not consider switching cost functions. Readers can refer to Verscheure et al. (2009); Gong et al. (2006); Betts (1998) and references therein for detailed review of techniques in numerical methods of NCOCP.

This paper considers an NCOCP having a switching cost function, which is result from hardware limitations in prevailing factory automation systems. Although an NCOCP with a switching cost function might be put in the hybrid system framework and studied by hybrid maximum principle Sussmann (1999); Garavello and Piccoli (2005); Shaikh and Caines (2007), bi-level optimization scheme Vasudevan et al. (2012); Wardi and Egerstedt (2012), this paper uses the conventional Minimum Principle and the Optimal Principle instead, which is more natural. This is because the NCOCP studied in this paper has switches based on a function of state and control variables. This is different from the a vast of literatures in optimal control of hybrid systems where switches, represented by discrete-time inputs, are free to design. This paper is also substantially different from prior work Wang et al. (2012) by providing a more concise and rigorous derivation of necessary conditions, and including the analysis of structures of optimal trajectories, a novel decomposition-based algorithm to solve the resultant multi-point boundary value problems (MBVPs), and experimental results. The main contribution of this paper is two fold. First, this paper proposes a systematic method to derive necessary conditions for NCOCPs having switching cost functions. The proposed method is complementary to existing work. Second, this paper solves the energy optimal motion planning for a servomotor system using the proposed method and validates the effectiveness of this approach by simulations and experiments. Specifically, a key concept "sub-trajectory" is introduced to match each piece of the piecewise Hamiltonian defined according to the switching cost function. Necessary conditions of the optimal trajectory are established as a combination of necessary conditions of each sub-trajectory and the Weierstrass-Erdmann corner conditions between sub-trajectories. The complete set of feasible structures of optimal trajectories is studied on the basis of necessary conditions. Transitions between sub-trajectories are analyzed by using the Weierstrass-Erdmann corner condition, and transitions between arcs within each sub-trajectory are investigated through necessary conditions of the sub-trajectory. Feasible structures of optimal trajectories can be simply presented by various state transition diagrams, where each state represents either one sub-trajectory or arc. The identified set of feasible structures has a finite number of elements, thus eliminates the major handicap in applying indirect methods to this problem. A decomposition-based shooting algorithm is proposed to solve the resultant MBVPs to compute the optimal trajectory. Simulations and experiments are also performed to validate the design methodology and energy saving benefits. While it is well-understood the difficulty to compute optimal solutions of complex NCOCPs from necessary conditions, the methodology to establish such a set of necessary conditions for NCOCPs with switching cost function or dynamics is general and is of theoretical interest.

This paper is organized as follows. In Section 2, the trajectory planning is formulated as a nonlinear constrained optimal control problem. Section 3 presents the derivation of necessary conditions. Section 4 identifies the complete set of feasible structures of optimal trajectories. In Section 5, a decomposition-based shooting method is

presented to solve multi-point boundary value problems and various simulation examples show the effectiveness of the proposed design methodology and algorithm. Experimental results are provided in Section 6 to validate the methodology and energy saving benefit.

2 Preliminary

Consider the following second order servomotor model

$$I\ddot{\theta} = K_\tau u - \bar{c} - \bar{d}\dot{\theta},$$

where θ is the rotation angle of the motor, I is the sum of load and servo motor inertia, K_τ is the torque constant of the servo motor, $\bar{d}$ is the viscous friction coefficient, $\bar{c}$ is the Coulomb friction, and u is the input current. For low inertia servomotors, it is fair to model the Coulomb friction has a constant magnitude. Although the Coulomb friction changes its sign according to the velocity, this is not considered here because of the introduction of non-negative velocity constraints. Given $x = (x_1, x_2)^T = (\theta, \dot{\theta})^T$, the plant model is written in the state space form

$$\begin{aligned} &\dot{x} = Ax + Bu + C, \\ &A = \begin{bmatrix} 0 & 1 \\ 0 & -d \end{bmatrix}, \quad B = \begin{bmatrix} 0 \\ b \end{bmatrix}, \quad C = \begin{bmatrix} 0 \\ -c \end{bmatrix}, \end{aligned} \tag{1}$$

where $d = \bar{d}/I, c = \bar{c}/I, b = K_\tau/I$. The real servomotor dynamics has minor nonlinearity due to saturation, hysteresis etc. Considering the Linear Time Invariant (LTI) model (1) is without loss of generality because the proposed methodology can be readily generalized to the nonlinear physical plant case.

2.1 Loss Models

A simple characterization of the energy consumption of servomotors is the copper loss, which is consistent with the following quadratic cost function

$$E(u) = \int_0^{t_f} u^2 \, \mathrm{d}t. \tag{2}$$

The loss model (2) may not be valid for certain types of motors, for instance, high speed or large power servomotors. This paper considers the energy consumption combining iron loss, switching loss of amplifiers, mechanical work, as well as copper loss, which is written as

$$P(x,u) = Ru^2 + K_e x_2^2 u^2 + K_h \left|x_2\right| |u|^\gamma + K_s \left|u\right| + K_\tau u x_2,$$

where R is the resistance of the servo motor, K_e and K_h are constant coefficients of eddy current and hysteresis losses, γ is the Steinmetz constant, and K_s is a constant coefficient of the switching loss. During the deceleration period, $P(x,u)$ could be negative. This means that the servomotor performs as a generator and converts the mechanical work into electricity. The generated electricity however cannot flow back to the utility grid. Thus we consider the minimization of the following cost functional for a servo system

$$\begin{aligned} E(x,u) &= \int_0^{t_f} Q(x(t),u(t)) \, \mathrm{d}t, \\ Q(x(t),u(t)) &= \max(0, P(x(t),u(t))), \end{aligned} \tag{3}$$

where t_f is the tracking time specified by users.

2.2 Problem Statement

The reference trajectory generation is treated as an open loop optimal control design problem as follows.

Problem 1 *Given the plant* (1)*, the initial state* $x(0) = x_0 = (0,0)^T$*, the final state* $x(t_f) = x_f = (r,0)^T$*, and the final time* t_f*, find the control* u^* *which minimizes the cost function* $E(x,u)$ *subject to acceleration and velocity constraints*

$$0 \le x_2 \le v_{max}, \quad |\dot{x}_2| \le a_{max}, \tag{4}$$

where $v_{\max}, a_{max}, r$ *are known constants.*

Problem 1 is reduced to time optimal trajectory planning if t_f is the minimal feasible tracking time. To simplify the presentation and focus on the energy optimal trajectory planning, we introduce the following assumption.

Assumption 2 *The final time* t_f *in Problem 1 is larger than the time optimal case.*

Control constraint, present in motion planning literatures e.g. Shin and Mckay (1985), is omitted in Problem 1 due to its similarity to acceleration constraint such that the presentation is simplified. On the other hand, max velocity and acceleration instead of control limitation are imposed as constraints because they generally appears as specifications of a servo system, and are more intuitive to customers. Problem 1 with the cost function (2) has been studied intensively. For instance, by including the tracking error penalty in (2), the model predictive control has been applied and leads to a quadratic programming problem. Since both the cost function and the constraints are convex, the resultant numerical optimization problem has a global minimum. This property however does not hold for Problem 1 with the cost function (3).

Numerous techniques have been proposed to treat inequality constraints, e.g. the integral penalty function approach considers the optimal control problem with a

new cost functional which penalizes heavily along trajectory violating constraints, relaxation approaches introduce slack variables to convert the inequality constraints into equality constraints. This paper adjoins inequality constraints to form the Lagrangian such that necessary conditions can be derived.

3 Conditions on Optimal Trajectories

Necessary conditions of an optimal trajectory for a state constrained optimal control problem have been investigated since 1960s. Sets of necessary conditions can be obtained in different ways. For instance, Jacobson et al. (1971), as an example of direct adjoining approach, establishes necessary conditions by directly adjoining the Hamiltonian to the state constraint in order to form the Lagrangian. This paper follows the same treatment of the state constraint as the indirect adjoining approach Pontryagin et al. (1962), where a state constraint is first converted into a mixed state control constraint, then the Lagrangian is formed by adjoining the Hamiltonian and the resultant mixed state control constraint. Interested readers are referred to Pesch (1994); Jacobson et al. (1971); Pontryagin et al. (1962); Hartl et al. (1995); A. E. Bryson, Jr. and Ho (1975) for details. For a state constraint, the following definition applies.

Definition 3 *A. E. Bryson, Jr. and Ho (1975) The one dimensional state constraint has an order of q if*

$$\begin{aligned} S^{(k)}(x) &= 0, \quad 0 \le k \le q-1, \\ S^{(q)}(x,u) &= 0, \end{aligned}$$

where $S^{(k)}(x)$ is computed by differentiating $S(x)$ k times with respect to time.

The velocity constraint in Problem 1 is a pure state constraint. We exemplify the utilization of indirect adjoining approach to convert $g_1(x) = x_2 - v_{max} \le 0$ into a mixed state control constraint. Taking time derivatives of $g_1(x)$ until the control u appears, we have $\dot{g}_1(x) = -dx_2 - c + bu$. Hence, $g_1(x) \le 0$ is equivalent to the formula: $-dx_2 - c + bu \le 0$, if $x_2 = v_{max}$, which prevents the trajectory from violating the constraint $g_1(x) \le 0$. The equivalent constraint of $g_2(x) = -x_2 \le 0$ can be similarly obtained. Thus the velocity constraint is converted into a mixed state control constraint as follows

$$\begin{aligned} \bar{g}_1(x,u) &= -dx_2 - c + bu \le 0, \text{ if } x_2 = v_{max} \\ \bar{g}_2(x,u) &= dx_2 + c - bu \le 0, \text{ if } x_2 = 0. \end{aligned} \tag{5}$$

Note two constraints in (5) cannot be active at the same time because the original state constraints $x_2 - v_{max} \le 0$ and $-x_2 \le 0$ cannot be active at the same time. The acceleration constraint is a mixed state control constraint

$$\begin{aligned} g_3(x,u) &= -dx_2 - c + bu - a_{max} \le 0 \\ g_4(x,u) &= -a_{max} + dx_2 + c - bu \le 0. \end{aligned} \tag{6}$$

The importance of existence conditions of optimal solutions for an optimal control problem was well received since 1960s. Representative work includes Filippov (1962); Cesari (1966). Combining the acceleration and velocity constraints, we know the control input u lies in a compact set

$$\begin{aligned} U(x) = \Big\{ u | & \frac{-a_{max} + dx_2 + c}{b} \le u \le \frac{a_{max} + dx_2 + c}{b}, \\ & \dot{g}_1(x) \le 0 \text{ if } g_1(x) = 0, \dot{g}_2(x) \le 0, \text{ if } g_2(x) = 0 \Big\} \end{aligned}$$

Problem 1 is a Pontryagin problem. We can further verify the Roxin's condition holds, i.e., for every (t, x), the set

$$\begin{aligned} N(x) = \big\{ (z^0, z) | & z^0 \ge Q(x,u), \\ & z = Ax + Bu + C, u \in U(x) \big\} \in \mathbb{R}^3 \end{aligned}$$

is a convex subset of $\mathbb{R}^3$. Given the compactness of $U(x)$ and the convexity of $N(x)$, (Cesari, 1966, Thm. 1) ensures the existence of optimal solutions.

3.1 Treatment of the Switching Cost Function

Non-differentiability of $Q(x,u)$ prevents us from a direct application of the Minimum Principle and its extended results. Given the switching cost function, we introduce notation of sub-trajectories

$$\begin{aligned} &\mathcal{S}_1 : \{t | P(t) > 0\}, \quad \mathcal{S}_1 = \mathcal{S}_{11} \cup \mathcal{S}_{12}, \\ &\mathcal{S}_{11} : \{t | P(t) > 0, u(t) > 0\}, \\ &\mathcal{S}_{12} : \{t | P(t) > 0, u(t) < 0\}, \\ &\mathcal{S}_2 : \{t | P(t) \le 0\}, \end{aligned}$$

and rewrite the cost function $E = \int_{\mathcal{S}_{11}} P(t)\,\mathrm{d}t + \int_{\mathcal{S}_{12}} P(t)\,\mathrm{d}t + \int_{\mathcal{S}_2} 0\,\mathrm{d}t$. By the Optimal Principle Bellman (1957), each sub-trajectory of $\mathcal{S}_{11}, \mathcal{S}_{12}$ and $\mathcal{S}_2$, which belongs to the entire optimal trajectory, is optimal. Thus necessary conditions of the entire optimal trajectory include necessary conditions of each sub-trajectory and junction conditions between sub-trajectories. Necessary conditions of each sub-trajectory can be established by applying the Minimum Principle on the Hamiltonian corresponding to the sub-trajectory. Introducing the notation of sub-trajectory also simplifies the determination of the set of feasible structures of optimal trajectories. Next we apply theorems in Hartl et al. (1995) to establish necessary conditions over different sub-trajectories of $\mathcal{S}_1, \mathcal{S}_2$ using corresponding Hamiltonian. Notation: H_1 and L_1 are the Hamiltonian and Lagrangian over $\mathcal{S}_1$; H_{11}, H_{12} and L_{11}, L_{12} are the Hamiltonian and the Lagrangian over $\mathcal{S}_{11}, \mathcal{S}_{12}$ respectively; and H_2 and L_2 are the Hamiltonian and Lagrangian over $\mathcal{S}_2$. To simplify presentation, we drop out the arguments in $H_{11}, H_{12}, H_1, H_2, H, L_{11}, L_1, L_{12}, L_2$.

3.2 Necessary Conditions over $\mathcal{S}_1$

Given $P(x,u) > 0$ and the mixed state control constraints (5)-(6), we take the following Hamiltonian

$$H_1 = P(x,u) + \lambda^T(Ax + Bu + C), \tag{7}$$

and the Lagrangian $L_1 = H_1 + \bar{H}_1$, where $\bar{H}_1 = \mu^T\mathcal{G}_v + \nu^T\mathcal{G}_a$ and $\mathcal{G}_v = [\bar{g}_1, \bar{g}_2]^T, \mathcal{G}_a = [g_3, g_4]^T$. Lagrange multipliers $\mu \in \mathbb{R}^2, \nu \in \mathbb{R}^2$ satisfy conditions

$$\begin{aligned} \mu^T\mathcal{G}_v = 0, \quad \mu \geq 0, \\ \nu^T\mathcal{G}_a = 0, \quad \nu \geq 0. \end{aligned}$$

Next we consider conditions on the optimal control.

3.2.1 Optimal Control

The Hamiltonian H_1 and the Lagrangian L_1 are not differentiable at $u = 0$. We express H_1 and L_1 piecewisely,

$$\begin{aligned} H_1 &= \begin{cases} H_{11} = P_1 + \lambda^T(Ax + Bu + C), & u > 0 \\ H_{12} = P_2 + \lambda^T(Ax + Bu + C), & u < 0, \end{cases} \\ L_1 &= \begin{cases} L_{11} = H_{11} + \bar{H}_1, & u > 0, \\ L_{12} = H_{12} + \bar{H}_1, & u < 0, \end{cases} \end{aligned} \tag{8}$$

where $P_1 = P(x,u)$ with $u > 0$, and $P_2 = P(x,u)$ with $u < 0$. We denote the positive control u_+ over $\mathcal{S}_{11}$

$$u_+ = \arg\min_{P>0, u>0} H_{11}, \tag{9}$$

and the negative control u_- over $\mathcal{S}_{12}$

$$u_- = \arg\min_{P>0, u<0} H_{12}. \tag{10}$$

Proposition 4 *Given $\gamma > 1$ and $x_2 \geq 0$, (9) has a unique solution u_+.*

Proof: Since $u > 0$ implies $P(x,u) > 0$, (9) is written as

$$u_+ = \arg\min_{0<u\leq u_{pacc}} H_{11},$$

where $u_{pacc} = (a_{max} + dx_2 + c)/b$ is the positive acceleration constrained control. If u_+ is on the boundary of its feasible domain, it is uniquely determined. Otherwise, given $\gamma > 1$, we verify that the Legendre-Clebsch condition holds over $\mathcal{S}_{11}$,

$$H_{11uu} = \frac{\partial^2 H_{11}}{\partial u^2} = 2R + 2K_e x_2^2 + \gamma(\gamma-1)K_h x_2 u^{\gamma-2} > 0.$$

Since the feasible control set is convex, and H_{11} is strictly convex, we conclude the uniqueness of u_+. ■

We have a similar proposition about u_-.

Proposition 5 *Given $\gamma > 1$ and $x_2 \geq 0$, (10) has a unique solution u_-.*

Assuming that at any time instant, only one constraint is active [1], then the control on constrained arcs is readily obtained as follows

$$u = \begin{cases} u_{vel}, & \text{velocity constraint is active,} \\ u_{pacc}, & \dot{x}_2 - a_{max} \leq 0 \text{ is active,} \\ u_{nacc}, & -a_{max} - \dot{x}_2 \leq 0 \text{ is active,} \end{cases} \tag{11}$$

where $u_{vel} = \frac{dx_2+c}{b}, u_{nacc} = \frac{-a_{max}+dx_2+c}{b}$.

3.2.2 Costate Dynamics

Since $x_2 \geq 0$, the partial derivative of L_1 w.r.t. x is well-defined. The costate dynamics are written as follows

$$\dot{\lambda} = -\frac{\partial L_1}{\partial x} \tag{12}$$

The costate variable is continuous at the entry point of the unconstrained arcs. For constrained arcs, we shall determine μ, ν and jump conditions of λ at their entry points. Since jumps of costate arise from interior points conditions, acceleration constraints will not incur discontinuity of the costate at the entry of acceleration constrained arcs A. E. Bryson, Jr. and Ho (1975). Denoting the entry time of an acceleration constrained arc as t_{entry}, the corresponding costate dynamics are written as (12) with $\mu = 0$ and ν solved from

$$L_{11u} = \frac{\partial L_{11}}{\partial u} = 0, \; g_3 = 0, \tag{13a}$$

$$L_{12u} = \frac{\partial L_{12}}{\partial u} = 0, \; g_4 = 0, \tag{13b}$$

and the entry condition $\lambda(t_{entry}^+) = \lambda(t_{entry}^-)$. Equation (13a) has a solution

$$\begin{aligned} \nu_1 = &\frac{-1}{b}\{2Ru + 2K_e x_2^2 u + \gamma K_h x_2 u^{\gamma-1} \\ &+ K_s + K_\tau x_2 + b\lambda_2\}. \end{aligned} \tag{14}$$

To ensure $\nu_1 \geq 0$, λ_2 should be negative. Equation (13b) has a solution

$$\begin{aligned} \nu_2 = &\frac{1}{b}\{2Ru + 2K_e x_2^2 u - \gamma K_h x_2 (-u)^{\gamma-1} \\ &- K_s + K_\tau x_2 + b\lambda_2\}. \end{aligned} \tag{15}$$

[1] This assumption is required to satisfy the constraint qualification (Hartl et al., 1995, (28)), which means the gradients of all active constraints w.r.t. u must be linearly independent. This assumption is generally true for considered servomotor systems.

On the other hand, the velocity constraint may incur jumps of the costate. Since the velocity constraint is an order one state constraint, it will not become active as a touch point, i.e., the velocity constraint is active over arcs. For the constraint $g_1 \leq 0$, we have jump conditions at the entry point of a velocity constrained arc

$$\begin{aligned} \lambda(t^+_{entry}) &= \lambda(t^-_{entry}) - \pi_1 \left(\frac{\partial g_1}{\partial x}\right)^T (t^-_{entry}) \\ H_{11}(t^+_{entry}) &= H_{11}(t^-_{entry}). \end{aligned} \tag{16}$$

where $\pi_1 \in \mathbb{R}$ is a Lagrange multiplier satisfying $\pi_1 \geq 0$ and $\pi_1 g_1 = 0$. Similarly, for the constraint $g_2 \leq 0$, jump conditions are

$$\begin{aligned} \lambda(t^+_{entry}) &= \lambda(t^-_{entry}) - \pi_2 \left(\frac{\partial g_2}{\partial x}\right)^T (t^-_{entry}), \\ H_{11}(t^+_{entry}) &= H_{11}(t^-_{entry}), \end{aligned}$$

where $\pi_2 \in \mathbb{R}$ is a Lagrange multiplier satisfying $\pi_2 \geq 0$ and $\pi_2 g_2 = 0$. The costate dynamics over a velocity constraint arc are written as (12) with $\nu = 0$. The Lagrange multiplier μ is determined from $L_{11u} = 0$ with $u = u_{vel} > 0$. We solve $L_{11u} = 0$ for

$$\begin{aligned} \mu_1 =& \frac{-1}{b}\{2Ru + 2K_e x_2^2 u + \gamma K_h x_2 u^{\gamma-1} \\ &+ K_s + K_\tau x_2 + b\lambda_2\}, \quad g_1 = 0 \\ \mu_2 =& \frac{-1}{b}\{2Ru + K_s + b\lambda_2\}, \quad g_2 = 0. \end{aligned} \tag{17}$$

where $u = u_{vel}$.

Remark 6 *When the velocity constraint is active, $u > 0$ and $P(x, u) > 0$. Hence, the velocity constrained arcs always belong to $\mathcal{S}_1$. Similarly, the arcs where the positive acceleration constraint $g_3 \leq 0$ is active belong to $\mathcal{S}_1$. For the negative acceleration constraint $g_4 \leq 0$, $u = u_{nacc}$ is generally negative, which may render $P(x, u) < 0$.*

3.3 Necessary Conditions over $\mathcal{S}_2$

Interval set $\mathcal{S}_2$ is characterized by the constraint $P(x, u) \leq 0$ which requires $u \leq 0$. According to Remark 6, over intervals $\mathcal{S}_2$, the Hamiltonian $H_2 = \lambda^T(Ax + Bu + C)$ and the Lagrangian $L_2 = H_2 + \bar{H}_1$ except $\mu = 0, \nu_1 = 0$, i.e., $L_2 = \lambda^T(Ax+Bu+C)+\nu_2 g_4$. The Lagrangian L_2 is differentiable w.r.t. x and u. The corresponding costate dynamics are

$$\begin{aligned} \dot{\lambda}_1 &= 0, \\ \dot{\lambda}_2 &= -\lambda_1 + d\lambda_2 - d\nu_2. \end{aligned} \tag{18}$$

For the case where the negative acceleration constraint is active over $\mathcal{S}_2$, we have

$$L_{2u} = \frac{\partial L_2}{\partial u} = b\lambda_2 - b\nu_2 = 0,$$

and solve $\nu_2 = \lambda_2$. The λ_2 dynamics is given by $\dot{\lambda}_2 = -\lambda_1$. Note the sign condition of ν_2 requires $\lambda_2 \geq 0$ when the negative acceleration constraint is active over $\mathcal{S}_2$.

For the unconstrained case, $\nu_2 = 0$, thus L_2 is written as

$$L_2 = H_2 = \lambda_1 + \lambda_2(dx_2 + c) + b\lambda_2 u.$$

It is clear that if $\lambda_2 \neq 0$, the optimal control is in the form of Bang-Bang. Otherwise, if $\lambda_2 \equiv 0$, we have a singular control arc. We have the following conclusion about the existence of singular arcs for Problem 1. Given Proposition 7, necessary conditions can be utilized to construct an optimal solution. Proposition 7 however does not establish the uniqueness of the optimal solution.

Proposition 7 *An optimal trajectory of Problem 1 does not include a singular arc.*

Proof: We assume that a singular arc exists, and try to derive a contradiction. Because the optimal control is uniquely defined over constrained arcs, we only need to consider the unconstrained arcs. Clearly sub-trajectories $\mathcal{S}_1$ do not include a singular arc. We only consider unconstrained arcs over $\mathcal{S}_2$, where the costate dynamics are

$$\begin{aligned} \dot{\lambda}_1 &= 0, \\ \dot{\lambda}_2 &= -\lambda_1 + d\lambda_2. \end{aligned} \tag{19}$$

The fact that $\lambda_2 \equiv 0$ over a singular arc and (19) implies $\lambda_1 \equiv 0$. Since $\dot{\lambda}_1 \equiv 0$, we know $\lambda_1 \equiv 0$ over $[0, t_f]$, and $\dot{\lambda}_2 = d\lambda_2$. Clearly, the singular arc cannot succeed a negative acceleration constrained arc or a negative unconstrained arc over $\mathcal{S}_2$ since both requires $\lambda_2 > 0$. If the singular arc is after $\mathcal{S}_{11}$, the Weierstrass-Erdmann corner condition between $\mathcal{S}_{11}$ and $\mathcal{S}_2$ requires λ_2 continuous at the transition time t_1, i.e., $\lambda_2(t_1^-) = 0$. However, given a non-positive λ_2, there does not exist a solution u_+ of (9). A contradiction is resulted thus $\mathcal{S}_{11}$ cannot precede the singular arc. Similarly, if a $\mathcal{S}_{12}$ precedes the singular arc, $\lambda_2(t_1^-) = 0$ gives a positive solution u_- of (10), and leads to a contradiction. Therefore, λ_2 cannot be zero at the entry of the singular arc. If λ_2 is non zero, it will not become zero over the entire arc due to its dynamics. The proof is completed. ■

We consider the case when $\lambda_2 = 0$ at finite points. Since $P(x, u) \leq 0$ allows a larger domain of admissible control than $P(x, u) \leq -\epsilon < 0$, the control over unconstrained arcs should be solved from

$$\arg\min_u H_2 \quad \text{subject to } P(x, u) \leq 0. \tag{20}$$

It can be shown that given $\gamma > 1, x_2 \geq 0$, the inequality $P(x,u) \leq 0$ gives a convex domain $D \subset \mathbb{R}^- \cup \{0\}$. Since H_2 is a linear function of u, (20) has a unique minimizer u_0. Given the domain D and the sign of λ_2, we have the unconstrained optimal control over $\mathcal{S}_2$

$$u_0 = \begin{cases} \min\{D\}, & \lambda_2 > 0, \\ \max\{D\} = 0, & \lambda_2 < 0. \end{cases} \tag{21}$$

3.4 Weierstrass-Erdmann Corner Conditions

Previously we established the necessary conditions of each sub-trajectory based on individual Hamiltonian. Here we derive junction conditions rising from switches among sub-trajectories $\mathcal{S}_{11}, \mathcal{S}_{12}$, and $\mathcal{S}_2$. These conditions are referred as the Weierstrass-Erdmann corner conditions Kirk (1970) and can be established by using calculus of variations. We exemplify the derivation of necessary conditions of the switch from $\mathcal{S}_{11}$ to $\mathcal{S}_{12}$.

Without loss of generality, we assume the switch from $\mathcal{S}_{11}$ to $\mathcal{S}_{12}$ happens at t_1 and simplify the cost

$$E = \int_0^{t_1} (L_{11} - \lambda\dot{x})\,\mathrm{d}t + \int_{t_1}^{t_f} (L_{12} - \lambda\dot{x})\,\mathrm{d}t.$$

Considering the variations $\delta t_1, \delta x, \delta\lambda, \delta u$, we have

$$\begin{aligned}
\delta E &= (L_{11} - \lambda\dot{x})(t_1^-)\delta t_1 + \int_0^{t_1} (\delta L_{11} - \dot{x}\delta\lambda - \lambda\delta\dot{x})\,\mathrm{d}t \\
&\quad - (L_{12} - \lambda\dot{x})(t_1^+)\delta t_1 + \int_{t_1}^{t_f} (\delta L_{12} - \dot{x}\delta\lambda - \lambda\delta\dot{x})\,\mathrm{d}t \\
&= (L_{11} - \lambda\dot{x})(t_1^-)\delta t_1 - (L_{12} - \lambda\dot{x})(t_1^+)\delta t_1 \\
&\quad - \lambda\delta x\Big|_0^{t_1^-} - \lambda\delta x\Big|_{t_1^+}^{t_f} + \int_0^{t_1^-} \underbrace{(\delta L_{11} - \dot{x}\delta\lambda + \dot{\lambda}\delta x)}_{\beta_1}\,\mathrm{d}t \\
&\quad + \int_{t_1^+}^{t_f} \underbrace{(\delta L_{12} - \dot{x}\delta\lambda + \dot{\lambda}\delta x)}_{\beta_2}\,\mathrm{d}t.
\end{aligned}$$

Since $x(t_f), x(0)$ are fixed, we have $\delta x(t_f) = 0, \delta x(0) = 0$. Also, Euler equation implies $\beta_1 = 0, \beta_2 = 0$. Given $\delta x(t_1^-) = \delta x^* - \dot{x}(t_1^-)\delta t$, and δx^* is arbitrary, the junction conditions at time t_1 are rewritten by

$$\begin{aligned}
(L_{11} - \lambda\dot{x} + \lambda\dot{x})(t_1^-) - (L_{12} - \lambda\dot{x} + \lambda\dot{x})(t_1^+) &= 0, \\
-\lambda(t_1^-) + \lambda(t_1^+) &= 0.
\end{aligned}$$

The junction conditions due to the transition from $\mathcal{S}_{11}$ to $\mathcal{S}_{12}$ at the switch time t_1 are given by

$$\begin{aligned}
H_{11}(t_1^-) &= H_{12}(t_1^+), \\
\lambda(t_1^-) &= \lambda(t_1^+).
\end{aligned} \tag{22}$$

Conditions of switches for other cases can be similarly obtained and take the same form as (22). The first equation in (22) not only infers that the piecewise Hamiltonian is continuous along the optimal trajectory, but also determines the switch time t_1. The second equation in (22), used in the proof of Proposition 7, implies the continuity of the costate variables during the transitions among sub-trajectories of $\mathcal{S}_{11}, \mathcal{S}_{12}$, and $\mathcal{S}_2$. The junction conditions (22) will be used extensively in Section 4 to determine structures of optimal trajectories. Given the continuity of state, (22) is equivalent to

$$P_1(t_1^-) - P_2(t_1^+) + b\lambda_2(t_1^-)(u(t_1^-) - u(t_1^+)) = 0. \tag{23}$$

3.5 Optimality

Previously we show (9), (10), and (20) has a unique minimizer respectively. Here we aim to show $\arg\min_{u\in U} H$ has a unique minimizer. We introduce notation

$$\begin{aligned}
&U_+ : U(x) \cap \mathbb{R}^+, \\
&D : [z_1, 0], \\
&D_{12} : \{U(x) \cap \mathbb{R}^-\} \setminus D,
\end{aligned}$$

where z_1 denotes the negative real root of $P(x,u) = 0$. If $P(x,u) = 0$ has only one real root, $z_1 = 0$. We have the following result on determining the optimal control.

Theorem 8 *Given the control set $U(x)$ and the piecewise Hamiltonian H, the formulae* $\arg\min_{u\in U} H$ *has a unique minimizer which takes the expression as follows*

$$u = \begin{cases} u_+, & u_+ \textit{is solvable from } (9), \\ u_-, & u_- \textit{is solvable from } (10), \\ u_0, & \textit{otherwise}. \end{cases} \tag{24}$$

Detailed proof of Theorem 8 is omitted due to space limitation. The key to show Theorem 8 is to verify the strict convexity of $Q(x,u)$ and the domain D_{12}, which is tedious but not difficult to establish. Theorem 8 not only excludes the possibility that both u_+ and u_- can be solved from (9) and (10) respectively, but also implies if $u_+ \in U_+$ is solved from (9), then

$$\min_{u\in U} H(u) = H_{11}(u_+) = \min_{u\in U_+} H_{11}(u);$$

if $u_- \in D_{12}$ is solved from (10), then

$$\min_{u\in U} H(u) = H_{12}(u_-) = \min_{u\in U_-} H_{12}(u);$$

if both u_+ and u_- cannot be solved from (9) and (10) respectively, then $\min_{u\in U} H = \min_{u\in D} H_2$.

4 Structures of Optimal Trajectories

We first analyze the order of sub-trajectories corresponding to $\mathcal{S}_{11}, \mathcal{S}_{12}$, and $\mathcal{S}_2$ respectively on the basis of the Weierstrass-Erdmann corner condition, then derive the structure of each sub-trajectory. We have the following main result.

Theorem 9 *An optimal solution of Problem 1 has the following properties:*

(I) the optimal trajectory always starts with a $\mathcal{S}_{11}$ type of sub-trajectory;
(II) a $\mathcal{S}_{11}$ type of sub-trajectory can be followed by a $\mathcal{S}_2$ type of sub-trajectory;
(III) a $\mathcal{S}_2$ type of sub-trajectory can be followed by a $\mathcal{S}_{12}$ type of sub-trajectory;
(IV) no other transitions between sub-trajectories are allowed.

Theorem 9 can be illustrated by a state transition diagram shown in Figure 1, where arrowed lines represent feasible transitions. Figure 1 means that only transitions from $\mathcal{S}_{11}$ to $\mathcal{S}_2$, and from $\mathcal{S}_2$ to $\mathcal{S}_{12}$ are allowed. Also the optimal trajectory always starts with a $\mathcal{S}_{11}$ type of sub-trajectory.

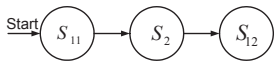

Fig. 1. State transition diagram between $\mathcal{S}_{11}, \mathcal{S}_2, \mathcal{S}_{12}$

Before proving Theorem 9, we first show the following proposition.

Proposition 10 *The costate λ_2 of the optimal trajectory of Problem 1 is either monotonically increasing or decreasing over a $\mathcal{S}_2$ type of sub-trajectory.*

Proof: We recall that the costate dynamics over a $\mathcal{S}_2$ type of sub-trajectory, denoted by S_2, is written as follows

$$\dot{\lambda}_1 = 0,$$
$$\dot{\lambda}_2 = \begin{cases} -\lambda_1 + d\lambda_2, & \text{unconstrained arcs,} \\ -\lambda_1, & \text{negative acceleration constrained arcs.} \end{cases} \tag{25}$$

In the beginning of S_2, if $-\lambda_1(t_1) + d\lambda_2(t_1) < 0$, then $\dot{\lambda}_2 < 0$ over the entire S_2, i.e., λ_2 monotonically decreases. If $-\lambda_1(t_1) + d\lambda_2(t_1) > 0$, then $\dot{\lambda}_2 > 0$ over the entire S_2, i.e., λ_2 monotonically increases. For negative acceleration constrained arcs, we already show λ_1 cannot be zero in the proof of Proposition 7. Hence, we have λ_2 monotonically increases if $\lambda_1 < 0$, decreases if $\lambda_1 > 0$. This completes the proof of the proposition. ■

Next we provide the proof of Theorem 9.

Proof: Proof of (I). An optimal trajectory cannot begin with a $\mathcal{S}_{12}$ type of sub-trajectory because the deceleration over $\mathcal{S}_{12}$ at the initial time leads to a negative velocity, thus the velocity constraint is violated. Alternatively, if the optimal trajectory begins with a $\mathcal{S}_2$ type of sub-trajectory, the velocity constraint will not be violated only if the plant maintains zero velocity over the entire $\mathcal{S}_2$ sub-trajectory. Such a trajectory which does not make full use of tracking time is not energy optimal. [2]

Proof of (II). Assume that a $\mathcal{S}_{11}$ type of sub-trajectory S_{11} is part of the optimal trajectory, and the sub-trajectory is followed by other sub-trajectories. We denote a $\mathcal{S}_{12}$ and a $\mathcal{S}_2$ type of sub-trajectories as S_{12}, S_2 respectively. Sub-trajectories S_{11}, S_2, S_{12} correspond to Hamiltonian H_{11}, H_2, H_{12} respectively. Contradiction is used to show that S_{11} cannot be followed by S_{12}. Assume that $\mathcal{S}_{11}$ is followed by S_{12}. The Weierstrass-Erdmann corner condition between S_{11} and S_{12} is written as (22), where t_1 is the transition time from S_{11} to S_{12}. From $\lambda_2(t_1^-) = \lambda_2(t_1^+)$ and the continuity of state at t_1, we can verify that $0 \le u_+(t_1^-) \le u_-(t_1^+)$, where u_+ and u_- are solved from (9) and (10) respectively. This contradicts the fact that S_{12} is a type of $\mathcal{S}_{12}$. Hence, a $\mathcal{S}_{11}$ type of sub-trajectory S_{11} can only be followed by a $\mathcal{S}_2$ type of sub-trajectory.

We next show (III). The Weierstrass-Erdmann corner condition between S_2 and S_{11} is used to derive a contradiction to show the claim (III). The Weierstrass-Erdmann corner condition between S_2 and S_{11} is written as follows

$$P_1(x,u) + b\lambda_2(t_1^+)u(t_1^+) = b\lambda_2(t_1^-)u(t_1^-), \tag{26}$$

where t_1 is the transition time from S_2 to S_{11}, and $\lambda_2(t_1^-) = \lambda_2(t_1^+)$. Equation (26) can be rewritten as

$$0 \le P(x,u) = b\lambda_2(t_1^-)(u(t_1^-) - u(t_1^+)).$$

Claim (I) means there exists a $\mathcal{S}_{11}$ switching to $\mathcal{S}_2$ at t_0, and $\lambda_2(t_0^-) = \lambda_2(t_0^+)$. By Proposition 10, if λ_2 increases over S_2, we know by the end of $\mathcal{S}_2$, $\lambda_2(t_1^+) > \lambda_2(t_0^+)$. Hence, the solution of (9), denoted by $u_+(t_1^+)$, is negative. This contradicts the fact that control over S_{11} has to be positive. On the other hand, if λ_2 decreases over S_2, we have $u(t_1^-) = 0$, and rearrange (26)

$$P_1(x,u) = -b\lambda_2(t_1^-)u(t_1^+), \quad u(t_1^+) > 0. \tag{27}$$

[2] Assume an optimal trajectory has a zero control over$[0, t_1]$, and a positive control over $[t_1, t_2]$. It is not difficult to construct a new trajectory with the positive control defined over $[t_1 - \delta t, t_2]$ based on the original trajectory and verify that the new trajectory yields a lower cost.

Equation (27) can be reduced to

$$Ru + K_e x_2^2 u + K_h x_2 u^{\gamma-1} + K_s + K_\tau x_2 + b\lambda_2 = 0,$$

which gives a solution $u(t_1^+) > u_+(t_1^+)$. A contradiction is derived, thus (III) is shown.

Proof of (IV). The proofs of (II) and (III) show that the transitions from S_{11} to S_{12}, and from S_2 to S_{11} are not allowed. We only need to show that another two transitions, from S_{12} to S_2, and from S_{12} to S_{11}, are impossible. We first assume the transition from S_{12} to S_2 at time t_1. The Weierstrass-Erdmann corner condition is written as

$$P_2(x,u) + b\lambda_2(t_1^-)u(t_1^-) = b\lambda_2(t_1^+)u(t_1^+), \qquad (28)$$

where $\lambda_2(t_1^-) = \lambda_2(t_1^+)$. We know $\lambda_2(t_1^-)$ is necessary positive to ensure (10) gives a negative solution. Since $u_-(t_1^-)$ from (10) is always greater than $u(t_1^-)$ satisfying (13b), the left hand side of (28) is non-negative. Meanwhile, since $\lambda_2(t_1) > 0$, we have $u(t_1^+) < 0$ over $\mathcal{S}_2$, and the right hand side is negative. A contradiction is derived, and the transition from S_{12} to S_2 is not allowed. To show that the transition from S_{12} to S_{11} at time t_1 is impossible, we also use contradiction. The Weierstrass-Erdmann corner condition is written as (22). Over S_{12}, $\lambda_2(t_1^-) > 0$, on the other hand, over S_{11}, $\lambda_2(t_1^+) < 0$. A contradiction to the Weierstrass-Erdmann corner condition is resulted. We therefore prove that the transition from S_{12} to S_{11} at time t_1 is impossible. ■

Applying Theorem 9 leads to the following conclusions.

Theorem 11 *An optimal trajectory of Problem 1 takes one of the following structures*

(I) a $\mathcal{S}_{11}$ type of sub-trajectory;
(II) a $\mathcal{S}_{11}$ type of sub-trajectory followed by a $\mathcal{S}_2$ type of sub-trajectory;
(III) a $\mathcal{S}_{11}$ type of sub-trajectory followed by a $\mathcal{S}_2$ type of sub-trajectory and a $\mathcal{S}_{12}$ type of sub-trajectory sequentially.

4.1 Structures of a Sub-Trajectory $\mathcal{S}_{11}$

Prior to showing the structure of the sub-trajectory $\mathcal{S}_{11}$, we first prove some useful results.

Proposition 12 *The optimal control over the sub-trajectory $\mathcal{S}_{11}$ is continuous.*

Proof: We have verified the Hamiltonian H_{11}, corresponding to $\mathcal{S}_{11}$, is convex in u, thus H_{11} is regular. From (Hartl et al., 1995, Lem. 4.3), one concludes the continuity of u. ■

Remark 13 *Similar to Proposition 12, one can show that the optimal control over the sub-trajectory $\mathcal{S}_{12}$ is continuous.*

The optimal control discussed in Section 3 implies that the $\mathcal{S}_{11}$ sub-trajectory could consist of three types of arcs: positive acceleration constrained arc S_{pa}^+, unconstrained positive control arc S_{pu}^+, and velocity constrained arc S_{pv}^+. We have the following proposition about the structure of the sub-trajectory $\mathcal{S}_{11}$.

Proposition 14 *The last arc of the sub-trajectory $\mathcal{S}_{11}$ has to be a unconstrained positive control arc;*

Proof: If the optimal trajectory only consists of the sub-trajectory $\mathcal{S}_{11}$, the last arc cannot be a velocity constrained arc since it violates the terminal state conditions. Also, the last arc cannot be a positive acceleration constrained arc in order to avoid the violation of the positive velocity constraint. This is because from the continuity of state and control contradictory, and the zero velocity condition at the final time, the positive acceleration control at the final time implies the existence of a left neighborhood $B^-(t_f,\epsilon) : \{t \in (t_f - \epsilon, t_f)\}$ such that the velocity in $B^-(t_f,\epsilon)$ is negative. This fact violates the velocity constraint.

If the optimal trajectory includes a $\mathcal{S}_2$ sub-trajectory, contradiction is used to show that only a unconstrained positive control arc can precede the sub-trajectory $\mathcal{S}_2$. Assume a positive acceleration constrained arc is the last arc of $\mathcal{S}_{11}$. The Weierstrass-Erdmann corner conditions between $\mathcal{S}_{11}$ and $\mathcal{S}_2$ are written as (22), which gives

$$P_1(t_1^-) + b\lambda_2(t_1^-)u(t_1^-) = b\lambda_2(t_1^+)u(t_1^+), \qquad (29)$$

where $\lambda_2(t_1^-)$ is clearly negative to ensure the positive acceleration constrained control. Thus $\lambda_2(t_1^+) < 0$, which, according to the established expression of the optimal control in $\mathcal{S}_2$, implies $u(t_1^+) = 0$. Hence, (29) is rewritten as follows

$$P_1(t_1^-) + b\lambda_2(t_1^-)u(t_1^-) = 0, \qquad (30)$$

which can be further reduced to

$$Ru + K_e x_2^2 u + K_h x_2 u^{\gamma-1} + K_s + K_\tau x_2 + b\lambda_2 = 0. \quad (31)$$

Denoting the optimal control solved from (31) as $u(t_1^-)$ and the optimal control solved from $H_{11u} = 0$ as $\bar{u}(t_1^-)$, and comparing (31) to $H_{11u} = 0$, we know $u(t_1^-) > \bar{u}(t_1^-) > u_{pacc}$. This is impossible because $\bar{u}(t_1^-)$ violates the acceleration constraint and $u(t_1^-)$ can be taken as the optimal control over the positive acceleration constrained arc. The contradiction means the last arc of $\mathcal{S}_{11}$ cannot be a positive acceleration constrained arc.

Assume a velocity constrained arc is the last arc of $\mathcal{S}_{11}$. Equations (30) and (31) also hold. We can solve λ_2 from (31) and substitute the solution into (17), and have

$$\begin{aligned}\mu_1 &= \frac{-1}{b}\{2Ru + 2K_e x_2^2 u + \gamma K_h x_2 u^{\gamma-1} + K_s + K_\tau x_2 - \\ &\quad (Ru + K_e x_2^2 u + K_h x_2 u^{\gamma-1} + K_s + K_\tau x_2)\} \\ &= \frac{-1}{b}\{Ru + K_e x_2^2 u + (\gamma-1) K_h x_2 u^{\gamma-1}\} < 0.\end{aligned}$$

The fact $\mu_1 < 0$ contradicts the necessary condition: $\mu_1 \geq 0$ over the velocity constrained arc. The proposition is shown. ■

It is quite difficult to derive a complete list of feasible structures of sub-trajectory $\mathcal{S}_{11}$ for Problem 1 with (3). We consider a simplified cost function to get more elegant results. For the rest of paper, we consider Problem 1 with the following simplified cost function, though some results still hold for Problem 1 with (3)

$$E = \int_0^T \max(0, Ru^2 + K_s|u| + K_\tau x_2 u)\,\mathrm{d}t. \tag{32}$$

Theorem 15 *An $\mathcal{S}_{11}$ type of sub-trajectory, which is a part of an optimal solution of Problem 1 with the cost function* (32)*, only admits the following transitions between arcs:*

(I) from a positive acceleration constrained arc S_{pa}^+ to a unconstrained control arc S_{pu}^+;
(II) from a unconstrained control arc S_{pu}^+ to a velocity constrained arc S_{pv}^+;
(III) from a velocity constrained arc S_{pv}^+ to a unconstrained control arc S_{pu}^+.

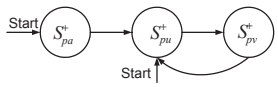

Fig. 2. State transition diagram between arcs in $\mathcal{S}_{11}$

Theorem 15 can be illustrated by the state transition diagram in Figure 2. A sub-trajectory $\mathcal{S}_{11}$ can start with S_{pa}^+ or S_{pu}^+, but can only exit from S_{pu}^+. We readily know that a $\mathcal{S}_{11}$ sub-trajectory can only have at most one S_{pa}^+. On the other hand, the loop between S_{pu}^+ and S_{pv}^+ requires further analysis.

Proof: A sub-trajectory $\mathcal{S}_{11}$ could consist of three types of arcs, which yields 6 possible transitions. Theorem 15 includes three possible transitions. We therefore use contradiction to show that the other three transitions are impossible. Clearly we can verify that the transitions between positive acceleration constrained and velocity constrained arcs are impossible because the discontinuity of control at the transition time is resulted.

We next focus on the derivation of a contradiction if a transition from unconstrained control arc to positive acceleration constrained arc is assumed at time t_1. Consider the costate dynamics over a unconstrained control arc as in (12), where $\mu = \nu = 0$. Since ν_1 is taken s.t. (13a) holds, and the unconstrained control at t_1 satisfies $H_{11u} = 0$, we have $\nu_1(t_1) = 0$. Hence, $\dot{\lambda}_2(t_1)$ is continuous. Next we show at t_1,

$$\dot{\lambda}_2(t_1) < \rho = -\frac{1}{b}\left(\frac{da_{max}R}{b} + K_\tau a_{max}\right). \tag{33}$$

Since the optimal control at t_1 also satisfies $H_{11u} = 0$ which is obviously continuous differentiable, we take its time derivative and have $R\dot{u} + K_\tau \dot{x}_2 + b\dot{\lambda}_2 = 0$. The time derivative of u at t_1 is written as

$$\dot{u} = -\frac{K_\tau \dot{x}_2 + b\dot{\lambda}_2}{R}. \tag{34}$$

From (34), we know $\dot{u}(t_1) > \dot{u}_{pacc} = da_{max}/b$, otherwise, no switch from the unconstrained arc to the positive acceleration constrained arc could happen. This requires

$$\dot{\lambda}_2(t_1) \leq \rho < 0. \tag{35}$$

As we shown previously, the positive acceleration constrained arc has to switch to another positive unconstrained control arc. Assume this switch happens at time t_2, with $t_2 > t_1$. The switch from a positive acceleration constrained arc to a positive unconstrained arc happens because $\dot{u}(t_2) \leq \dot{u}_{pacc}$, where $u(t_2)$ satisfies $H_{11u} = 0$. Similarly, we have

$$\dot{\lambda}_2(t_2) \geq \rho < 0. \tag{36}$$

Combining (35) and (36), we have

$$\dot{\lambda}_2(t_2) \geq \dot{\lambda}_2(t_1), \tag{37}$$

which is the necessary condition to enable to switches from positive unconstrained arc to positive acceleration constrained arc at t_1, and from positive acceleration constrained arc to positive unconstrained arc at t_2. On the other hand, it is straightforward to verify $u(t_2) > u(t_1)$. Combining the fact that $x_2(t_2) > x_2(t_1)$, the costate dynamics (12) at t_1, t_2 implies $\dot{\lambda}_2(t_2) < \dot{\lambda}_2(t_1)$. This contradicts (37). We therefore prove the switch from a positive unconstrained arc to a positive acceleration constrained arc is impossible. ■

Proposition 16 *An optimal sub-trajectory $\mathcal{S}_{11}$ comprises at most one velocity constrained arc.*

Proof: Assuming there exists a switch from a velocity constrained arc to a positive unconstrained control arc at t_1, we need to show there does not exist a switch from

the positive unconstrained control arc to another velocity constrained arc at $t_2 > t_1$. We have the time derivative of $H_{11u} = 0$ as in (34). Also, we have $\dot{x}_2(t_1) \leq 0$, otherwise the velocity constraint will be violated over the succeeding unconstrained arc. Due to the interior point constraints, we also know that at the exit point of the velocity constrained arc, the velocity trajectory has to be tangential which means $\dot{u}(t_1) = 0$. Hence, we know $\dot{\lambda}_2(t_1) \geq 0$. But $\dot{x}_2$ cannot remain zero over unconstrained arc, because $\dot{x}_2 = 0$ means the trajectory is still on the velocity constrained arc. Hence, $\dot{x}_2$ becomes negative in the neighborhood $B(t_1, \epsilon) : t_1 < t < t_1 + \epsilon, \epsilon > 0$. Combining this observation with the costate dynamics over unconstrained arc, we know $\dot{\lambda}_2(t) > \dot{\lambda}_2(t_1)0$ for time $t > t_1$ since $2K_2x_2u^2 + K_h|u|^\gamma + K_\tau u$ decreases as x_2 decreases. $\dot{\lambda}_2(t) > 0$ over the positive unconstrained arc implies $\lambda_2(t) > \lambda_2(t_1)$. Given $\lambda_2(t) > \lambda_2(t_1)$, it is impossible to have $u(t)$ over the positive unconstrained arc s.t. $u(t) = u_{vel}$. ■

Given Theorem 15 and Proposition 16, we are able to establish the set of feasible structures of $\mathcal{S}_{11}$.

Theorem 17 *Given a $\mathcal{S}_{11}$ sub-trajectory as a part of an optimal trajectory of Problem 1 with the cost functional* (32)*, its structure must belong to the following set*

(I) a positive unconstrained arc;
(II) a positive acceleration constrained arc followed by a positive unconstrained arc;
(III) a positive unconstrained arc followed by a velocity constrained arc and a positive constrained arc;
(IV) a positive acceleration constrained arc followed by a positive unconstrained arc and a velocity constrained arc and a positive unconstrained control arc.

4.2 Structures of a Sub-Trajectory $\mathcal{S}_2$

As shown in Section 3, a sub-trajectory $\mathcal{S}_2$ can include three types of arcs: zero control arc S_0^-, negative acceleration constrained arc S_{na}^-, and negative unconstrained control arc S_{nu}^-. Following Proposition 14, we have the following observation about the structure of $\mathcal{S}_2$.

Proposition 18 *A sub-trajectory $\mathcal{S}_2$ always begins with a zero control arc.*

Proof: Proposition 14 shows $\mathcal{S}_{11}$ ends with a positive unconstrained control arc. Assume the transition time is t_1. We have $\lambda_2(t_1^-) \leq 0, u(t_1^-) \geq 0$, and $P_1(t_1^-) \geq 0$. Meanwhile, the optimal control over $\mathcal{S}_2$ is non-positive, i.e., $u(t_1^+) \leq 0$. Given these facts, the switching condition between $\mathcal{S}_{11}$ and $\mathcal{S}_2$, denoted by (29), holds if and only if $u(t_1^-) = u(t_1^+) = 0$. Proposition is shown. ■

Proposition 18 allows us to enumerate the complete list of possible structures of a $\mathcal{S}_2$ type sub-trajectory.

Theorem 19 *Assume the optimal solution of Problem 1 comprises of a $\mathcal{S}_2$ sub-trajectory. The $\mathcal{S}_2$ sub-trajectory must take one of the following structures*

(I) a zero control arc;
(II) a zero control arc followed by a negative accelerations constrained arc;
(III) a zero control arc followed by a negative unconstrained control arc;
(IV) a zero control arc followed by a negative acceleration constrained arc and a negative unconstrained control arc respectively;

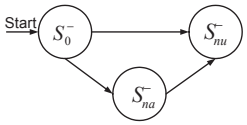

Fig. 3. State diagram of transitions between arcs in $\mathcal{S}_2$

Theorem 19 can be summarized by the state transition diagram in Figure 3, where three types of transitions are allowed. Proof of Theorem 19 is omitted because of space limitation and the similarity to that of Theorem 15.

4.3 Structures of a Sub-Trajectory $\mathcal{S}_{12}$

A sub-trajectory $\mathcal{S}_{12}$ can include two types of arcs: negative unconstrained control arc S_{nu}^+, and negative acceleration constrained arc S_{na}^+. Similar to the structure analysis of $\mathcal{S}_{11}$, we consider Problem 1 with the simplified cost functional (32). We have the following result about the structure of a sub-trajectory $\mathcal{S}_{12}$.

Theorem 20 *Assume the optimal solution of Problem 1 with the cost function* (32) *comprises of a $\mathcal{S}_{12}$ sub-trajectory. The $\mathcal{S}_{12}$ sub-trajectory must take one of the following structures*

(I) a negative unconstrained control arc;
(II) a negative unconstrained control arc followed by a negative acceleration constrained arc;
(III) a negative acceleration constrained arc.

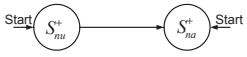

Fig. 4. State diagram of transitions between arcs in $\mathcal{S}_{12}$

Theorem 20 can be summarized by the state transition diagram in Figure 4. Proof of Theorem 20 is omitted because of space limitation and the similarity to that of Theorem 15.

5 Computation of Optimal Trajectories

Section 3 establishes necessary conditions as a set of ordinary differential equations and nonlinear algebraic

equations which are piecewisely defined. Given the structure of the optimal trajectory, necessary conditions can be formulated a Multi-Point Boundary Value Problem (MBVP). Section 4 analyzes the feasible structures of optimal trajectories for Problem 1 with the cost functional (32), which enables the use of indirect methods for this particular problem. Since there are only finite number of elements in the structure set, it is not expensive to identify the structure of the optimal trajectory by either performing exhaustive enumeration or iterative active-set type of searches. Hence, this section only concentrates on a customized algorithm to solve an MBVP, i.e., the knowledge of the structure of the optimal trajectory is assumed and the MBVP to be solved is well-defined. Interested readers are referred to Ascher et al. (1987); Pesch (1994) for details about MBVPs.

5.1 A Decomposition-Based Shooting Algorithm

An MBVP can be effectively solved by multiple shooting methods Bock and Plitt (1984); Pasic (1999); Fraser-Andrews (1999). A shooting algorithm generally includes defining parameters and boundary conditions, generating initial guess of parameters, and iteratively updating parameters until boundary conditions are satisfied. Different techniques are proposed to update parameters e.g. Newton methods Nocedal and Wright (2006), continuation method Ohtsuka (2004). Compared to conventional multiple shooting methods, the proposed method introduces a different parameterization scheme of MBVPs, and a decomposition-based algorithm to update parameters. As for the parameterization, we only treat the state and costate values at switches between arcs and switch times as parameters. Thus the proposed method is a mix of single and multiple shooting methods. The goal of this parameterization is to reduce the computation load by reducing the number of parameters. Clearly, the proposed parameterization scheme scarifies the convergence property compared to conventional multiple shooting methods, for instance, more sensitive to initial guesses. This motivates the decomposition-based parameter update algorithm given in Figure 5.

The proposed parameter update algorithm relies on the partition of parameters into at least two sets. Similarly, boundary conditions are partitioned into at least two sets. A typical choice of parameter partition scheme is: take the state and costate values as the first set, and switch times as the second set. Accordingly, the first set of boundary conditions is chosen to update the first set of parameters, and generally comprises the continuity conditions of state and costate; the second set of boundary conditions is used to update switch times, and usually comprises of continuity conditions of control, the Weierstrass-Erdmann corner condition etc. Introducing decomposition technique is based on the realization that boundary conditions are much more sensitive to switch

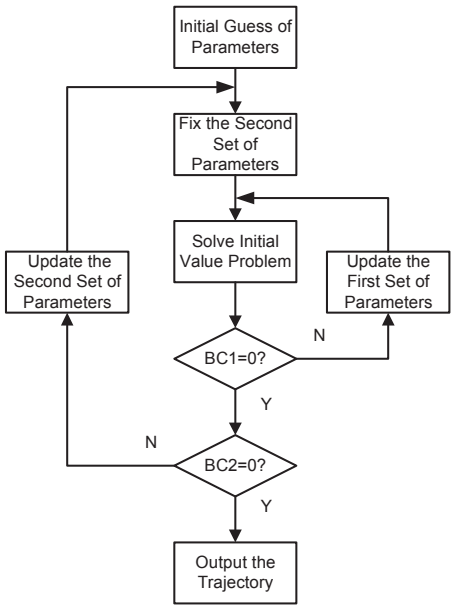

Fig. 5. the decomposition-based algorithm

times, thus it is desirable to remove the coupling-effect of bad state and costate initial guess before adjusting switch times. Simulation shows the decomposition enjoys much better convergence property than the conventional one-step parameter update algorithm. As a comparison, a solver using conventional parameter update algorithm fails to converge at most cases.

5.2 Simulation

We implemented the decomposition-based algorithm to generate the optimal trajectory of Problem 1 with the cost functional (32). Simulation results are shown in Figures 6–9. Figure 6 shows the optimal trajectory for case 1, which includes 5 arcs: positive acceleration constrained arc, positive unconstrained arc, zero control arc, negative unconstrained arc, and negative acceleration constrained arc. Figure 7 shows the optimal trajectory with 7 arcs. Figure 8 shows the optimal trajectory with a velocity constrained arc and other 5 arcs. Figure 9 shows various control trajectories over iterations to determine the structure of the optimal trajectory. Each control trajectory is obtained by solving a particular MBVP at each iteration. The structure candidate of the control trajectory for next iteration will be updated by checking constraints along the computed control trajectory, then the algorithm will solve a new MBVP corresponding to the updated structure in the next iteration. The computation time for all cases are within 1 second. We benchmark the proposed algorithm and several prevailing direct methods. The proposed solver gives much more accurate solutions, and achieves at least 10 times faster computation.

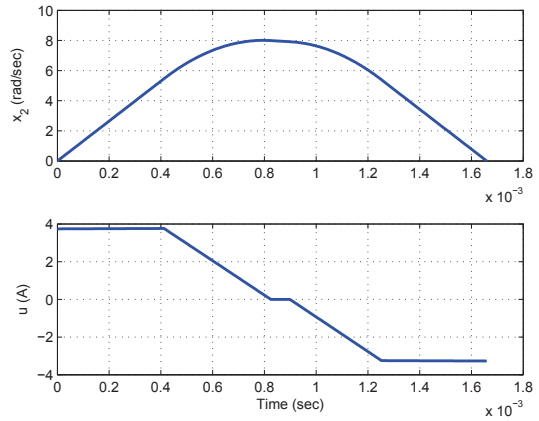

Fig. 6. Case 1: the trajectories of control and velocity

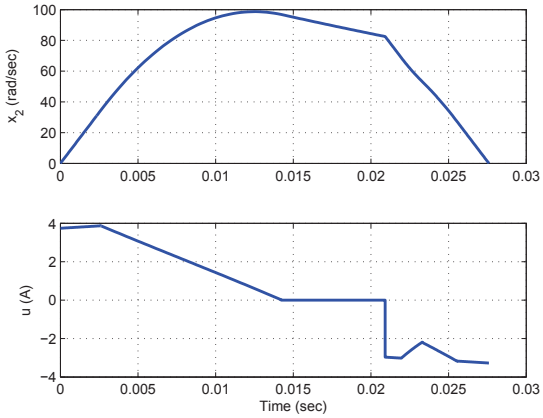

Fig. 7. Case 2: the trajectories of control and velocity

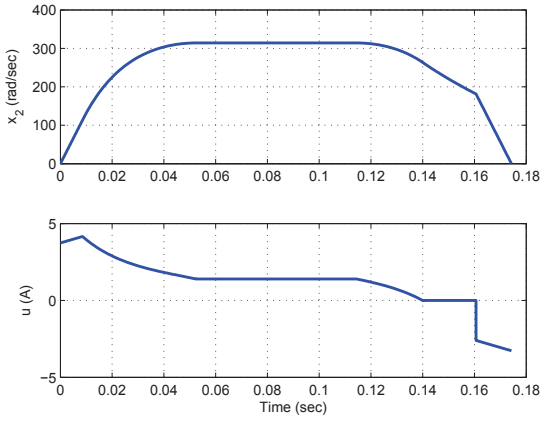

Fig. 8. Case 3: the trajectories of control and velocity

6 Experiments

The energy-saving performance of the optimal trajectory is verified on a motion control system comprising

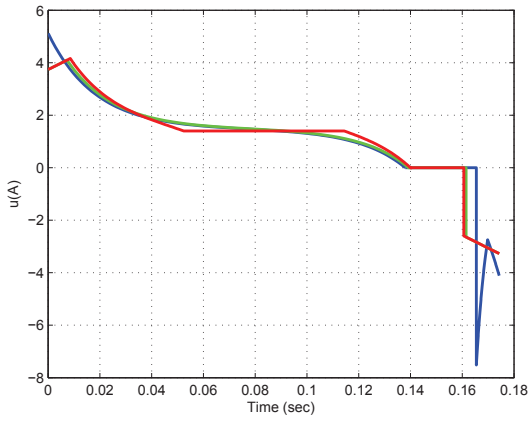

Fig. 9. Iterations to determine the structure of u for Case 3. Blue solid: no constraint; Green solid: acceleration constraint; Red solid: all constraints considered.

of a Mitsubishi Electric's AC servomotor HF-MP43K, an amplifier MR-J3-40A1, dSPACE ACE Kit 1104, and Matlab/Simulink. The experimental system is illustrated by the block diagram shown in Figure 10, where x_1^* is the position trajectory, $x_{1r}, \dot{x}_{1r}, \ddot{x}_{1r}$ are the reference position, velocity, and acceleration for a servomotor to track, and x_1, x_2 are the measured position and velocity of the servomotor. A position trajectory x_1^* is

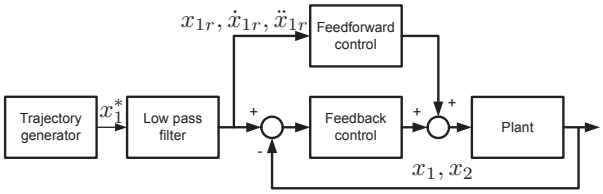

Fig. 10. the schematics of the experimental system

first generated given a motion positioning task data. A low pass filter processes x_1^* and produces the reference position, velocity, and acceleration signals. Filtering the trajectory x_1^* helps to reduce the tracking error as well as attenuate the vibration of the servomotor due to the non-smoothness in the acceleration trajectory. The tracking controller is composed of a feed-forward controller and a feedback controller. The amplifier MR-J3-40A1 works in the torque control mode, thus receives torque command from the tracking controller, and drives the servomotor with a flexible inertia load. The voltage and current inputs to the amplifier are measured to calculate the energy consumption of the entire motion control system. The dSPACE interfaces with the amplifier and the servomotor through AI/AO ports. The dSPACE operates at a sampling frequency of 10kHz. The energy efficiency of the motion control system using an optimal trajectory is experimentally validated by comparing to the case where a conventional trajectory is used. The conventional trajectory

is computed according to the method in Dodds (2008). Figure 11 shows the reference velocity and control trajectories of the servomotor for both cases, and Figure 12 shows the measured velocity and control trajectories of the servomotor. The energy trajectories for both cases shown in Figure 13 demonstrate that in the end of the tracking task, the optimal case saves more than 10% energy compared to the conventional case. Note that the energy consumption plots in Figure 13 exhibit periodic oscillation which inherits from the AC power source. The periodic oscillation is further illustrated by Figure 14 which shows time plots of voltage and current inputs to MR-J3-40A1 for both cases. The main takeout from experiment is that the optimal trajectory reduces the energy consumption from two aspects: first, smooth acceleration/deceleration; second, recycle of the regenerative energy as much as possible to brake the servomotor system.

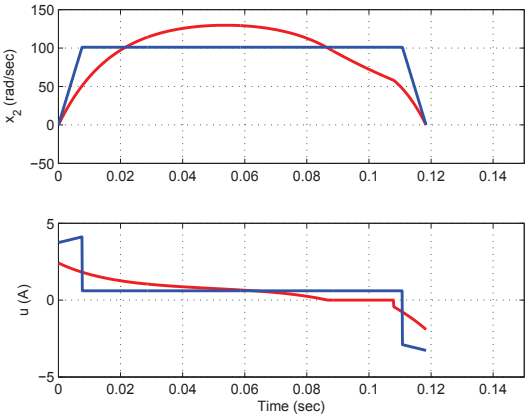

Fig. 11. the reference trajectories of controls and velocities. Blue: conventional case; Red: optimal case.

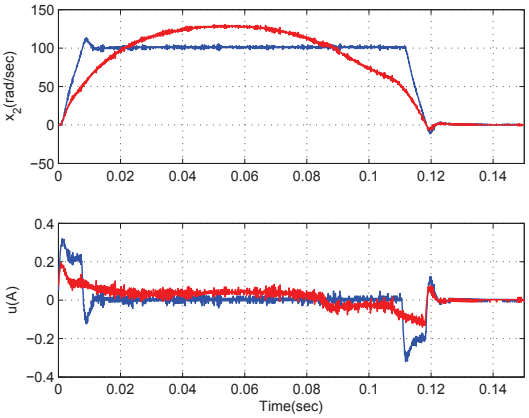

Fig. 12. the measured trajectories of controls and velocities. Blue: conventional case; Red: optimal case.

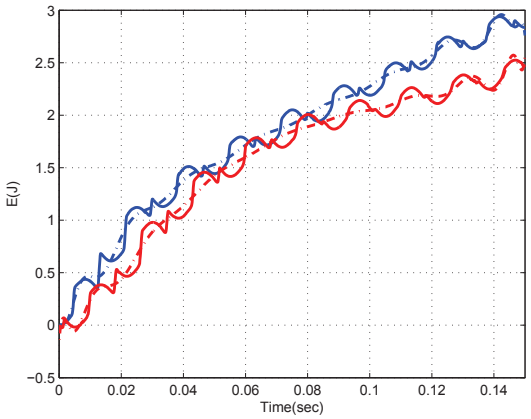

Fig. 13. the energy consumption curves: Blue solid: conventional case (measured data); blue dash dot: conventional case (curve fit); red solid: optimal case (measured data); red dash dot: optimal case (curve fit).

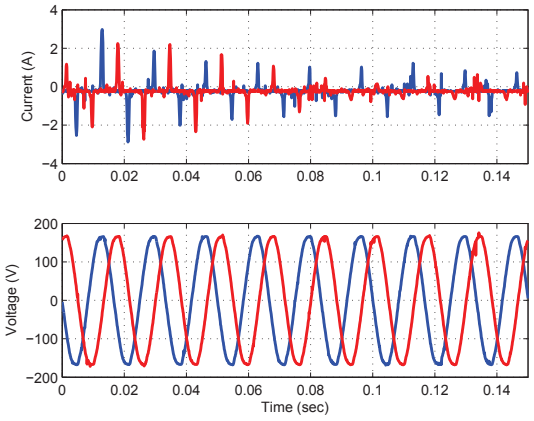

Fig. 14. the voltage and current curves: Blue solid: conventional case; red solid: optimal case.

7 Conclusion

This paper discussed the energy optimal trajectory generation of servomotor systems. Due to the switching cost function, necessary conditions were established as a combination of conditions over each sub-trajectories and the Weierstrass-Erdmann corner condition between sub-trajectories. The complete set of feasible structures of optimal trajectories were derived and illustrated as various state transition diagrams. A decomposition-based shooting algorithm was proposed to solve resultant multi-point boundary value problems. Simulation and experiment validated the design methodology and the energy efficiency.

References

A. E. Bryson, Jr. and Ho, Y.-C. (1975). *Applied Optimal Control: Optimization, Estimation, and Control*. Taylor & Francis Group, NY.

Abrahamsen, F., Blaabjerg, F., Pedersen, J., Grabowski, P., and Thogersen, P. (1998). On the energy optimized control of standard and high-efficiency induction motors in ct and hvac applications. *IEEE Trans. Ind. Appl.*, 34(4):822 –831.

Ascher, U. M., Mattheij, R. M. M., and Russell, R. D. (1981). Collocation software for boundary-value odes. *ACM Trans. Math. Software*, 7(2):209–222.

Ascher, U. M., Mattheij, R. M. M., and Russell, R. D. (1987). *Numerical Solution of Boundary Value Problems for Ordinary Differential Equations*. SIAM.

Bellman, R. E. (1957). *Dynamics Porgramming*. Princeton, NJ: Princeton University Press.

Betts, J. T. (1998). Survey of numerical methods for trajectory optimization. *J. Guid. Control Dynam.*, 21(2):193–207.

Bobrow, J. E., Dubowsky, S., and Gibson, J. S. (1985). Time-optimal control of robotic manipulators along specified paths. *Int. J. Robot Res.*, 4(3):3–17.

Bock, H. G. and Plitt, K. J. (1984). A multiple shooting algorithm for direct solution of optimal control problems. In *Proceedings of the 9th IFAC World Congress*, pages 242–247, Budapest, Hungary.

Cesari, L. (1966). Existence theorems for optimal solutions in Pontryagin and Lagrange problems. *SIAM J. Control Optim.*, 3(3):475–498.

Chang, S. S. L. (1963). Minimum time control with multiple saturation limits. *IEEE Trans. Automat. Contr.*, AC-8(1):35–42.

Dodds, S. (2008). Sliding mode vector control of pmsm drives with minimum energy position following. In *13th Power Electronics and Motion Control Conference*, pages 2559–2566.

Elnagar, G., Kazemi, M. A., and Razzaghi, M. (1995). The pseudospectral legendre method for discretizing optimal control problems. *IEEE Trans. Automat. Contr.*, AC-40(10):1793–1796.

Fahroo, F. and Ross, I. M. (2000). Direct trajectory optimization by a chebyshev pseudospectral method. In *Proc. 2000 ACC*, pages 3860–3864, Chicago, IL.

Filippov, A. F. (1962). On certain questions in the theory of optimal control. *SIAM J. Control Optim.*, 1(1):76–84.

Fraser-Andrews, G. (1999). A multiple shooting technique for optimal control. *J. Optimiz. Theory App.*, 102(2):299–313.

Garavello, M. and Piccoli, B. (2005). Hybrid necessary principle. In *Proc. 44th CDC*, pages 723–728, Seville, Spain.

Gergaud, J. and Haberkorn, T. (2006). Homotopy method for minimum consumption orbit transfer problem. *ESAIM: Control, Optimization and Calculus of Variations*, 12:294–310.

Ghozzi, S., Jelassi, K., and Roboam, X. (2004). Energy optimization of induction motor drives. In *IEEE International Conference on Industrial Technology*, volume 2, pages 602 – 610.

Gong, Q., Kang, W., and Ross, I. M. (2006). A pseudospectral method for the optimal control of constrained feedback linearizable systems. *IEEE Trans. Automat. Contr.*, AC-51(7):1115–1129.

Hartl, R. F., Sethi, S. P., and Vickson, R. G. (1995). A survey of the maximum principles for optimal control problems with state constraints. *SIAM Review*, 37:181–218.

Jacobson, D. H., Lele, M. M., and Speyer, J. L. (1971). New necessary conditions of optimality for control problems with state-variable inequality constraints. *J. Math. Anal. Appl.*, 35:255–284.

Kim, C. H. and Kim, B. K. (2007). Minimum-energy translational trajectory generation for differential-driven wheeled mobile robots. *J. Intell. Robot Syst.*, 49(4):367–383.

Kirk, D. E. (1970). *Optimal Contorl Theory: An Introduction*. Englewood Cliffs, NJ: Prentice-Hall.

La-orpacharapan, C. and Pao, L. Y. (2004). Shaped time-optimal feedback control for disk-drive systems with back-electromotive force. *IEEE Trans. Magn.*, 40(1):85–96.

Lambrechts, P., Boerlage, M., and Steinbuch, M. (2005). Trajectory planning and feedforward design for electromechnical motion systems. *Control Eng. Pract.*, 13:145–157.

Nocedal, J. and Wright, S. J. (2006). *Numerical Optimization*. Springer.

Ohtsuka, T. (2004). A continuation/GMRES method for fast computation of nonlinear receding horizon control. *Automatica*, 40(4):563–574.

Park, M.-H. and Won, C.-Y. (1991). Time optimal control for induction motor servo system. *IEEE Trans. Power Electron.*, 6(3):514–524.

Pasic, H. (1999). Multipoint boundary value solution of two point boundary value problem. *J. Optimiz. Theory App.*, 100(2):397–416.

Pesch, H. J. (1989). Real-time computation of feedback controls for constrained optimal control problems part 1: Neighboring extremals. In *Optimal Control Applications & Methods*.

Pesch, H. J. (1994). A practical guide to the solution of real-life optimal control problems. *Control and Cybernetics*, 23:7–60.

Pontryagin, L., Boltyanskii, V., Gamkrelidze, R., and Mischenko, E. (1962). *The Mathematical Theory of Optimal Processes*. Wiley-Interscience, New York.

Richards, A. and How, J. (2003). Model predictive control of vehicle maneuvers with guaranteed completion time and robust feasibility. In *Proc. 2003 ACC*, pages 4034–4040, Maui,HI.

Shaikh, M. S. and Caines, P. E. (2007). On the hybrid optimal control problem theory and algorithms. *IEEE Trans. Automat. Contr.*, AC-52(9):1587–1602.

Sheta, M. A., Agarwal, V., and Nataraj, P. S. V. (2009). A new energy optimal control scheme for a separately

excited dc motor based incremental motion drive. *International Journal of Automation and Computing*, 6(3):267–276.

Shiller, Z. and Lu, H.-H. (1992). Computation of path constrained time optimal motions with dynamic singularities. *Trans. ASME, J. Dyn. Sys. Meas. Control*, 114:34–40.

Shim, D., Kim, H., and Sastry, S. (2003). Decentralized nonlinear model predictive control of multiple flying robots. In *Proc. 42nd CDC*, pages 3621–3627, Maui,HI.

Shin, K. G. and Mckay, N. D. (1985). Minimum-time control of robotic manipulators with geometric path constraints. *IEEE Trans. Automat. Contr.*, AC-30(6):531–541.

Shin, K. G. and Mckay, N. D. (1986). A dynamic programming approach to trajectory planning of robotic manipulators. *IEEE Trans. Automat. Contr.*, AC-31(6):491–500.

Singh, L. and Fuller, J. (2001). Trajectory generation for a UAV in urban terrain, using nonlinear MPC. In *Proc. 2001 ACC*, pages 2301–2308, Arlington, VA.

Singh, S. and Leu, M. C. (1987). Optimal trajectory generation for robotic manipulators using dynamics programming. *Trans. ASME, J. Dyn. Sys. Meas. Control*, 109:88–96.

Sussmann, H. J. (1999). A maximum principle for hybrid optimal control problems. In *Proc. 38th CDC*, pages 425–430, Phoenix, AZ.

Toacse, G. and Culpi, W. (1976). Time-optimal control of a stepping motor. *IEEE Trans. Ind. Electron. Contr. Instrum.*, IECI-23(3):291 –295.

Trzynadlowski, A. (1988). Energy optimization of a certain class of incremental motion dc drives. *IEEE Trans. Ind. Electr.*, 35(1):60–66.

Vasak, M., Baotic, M., Petrovic, I., and Peric, N. (2007). Hybrid theory-based time-optimal control of an electronic throttle. *IEEE Trans. Ind. Electr.*, 54(3):1483 –1494.

Vasudevan, R., Gonzalez, H., Bajcsy, R., and Sastry, S. S. (2012). Consistent approximations for the optimal control of constrained switched systems. http://arxiv.org/abs/1208.0062.

Verscheure, D., Demeulenaere, B., Swevers, J., Schutter, J. D., and Diehl, M. (2009). Time-optimal path tracking for robots: A convex optimization approach. *IEEE Trans. Automat. Contr.*, AC-54(10):2318–2327.

Vittek, J., Bris, P., Skalka, I., Filka, R., Minarech, P., and Faber, J. (2010). Experimental verification of energy saving position control algorithm applied to the drives with pmsm. In *2010 14th International Power Electronics and Motion Control Conference (EPE/PEMC)*, pages S10–1 –S10–6.

Wang, Y., Ueda, K., and Bortoff, S. A. (2012). On the optimal trajectory generation for servomotors: a Hamiltonian approach. In *Proc. 51th CDC*, pages 7620–7625, Maui, HI.

Wardi, Y. Y. and Egerstedt, M. (2012). Algorithm for optimal mode scheduling in switched systems. In *Proc. 2012 ACC*, pages 4546–4551, Montreal, Canada.

Worrell, E., Bernstein, L., Roy, J., Price, L., and Harnisch, J. (2009). Industrial energy efficiency and climate change mitigation. *Energy Efficiency*, 2(2):109–123.

Zhao, Y., Wang, Y., Bortoff, S. A., and Ueda, K. (2013). Real-time energy-optimal trajectory generation for a servo motor. In *Proc. 2013 ACC*, pages 1167–1172, Washington, DC.